Appendices of *ColdBus*: A Near-Optimal Power Efficient Optical Bus

Eldhose Peter
Dept. of Computer Science and Engg
Indian Institute of Technology
Delhi - 110016
eldhose@cse.iitd.ac.in

Arun Thomas Anuj Dhawan
Dept. of Electrical Engg
Indian Institute of Technology
Delhi - 110016
{*eez138243,adhawan*}*@ee.iitd.ac.in*

Smruti R Sarangi
Dept. of Computer Science and Engg
Indian Institute of Technology
Delhi - 110016
srsarangi@cse.iitd.ac.in

APPENDIX A. PREDICTABILITY OF NETWORK BEHAVIOR

A. A Primer on Information Theory

Let us consider a random variable X that can take values in the discrete set $\mathcal{D}$. The entropy of X is defined as:

$$H(X) = -\sum_{d \in \mathcal{D}} p(d) log(p(d)) \tag{1}$$

$H(x)$ is a measure of the randomness of X. Let us assume that X is completely predictable. In this case, $H(X) = 0$. If it can randomly take any value in the set $\mathcal{D}$ with a uniform distribution, then the entropy is $log(\mid \mathcal{D} \mid)$. For the case of a binary random variable the entropy varies from 0 to 1. For example, a random variable representing the output of an unbiased coin has an entropy of 1.

The conditional entropy is defined as follows:

$$H(X|Y) = -\sum_{x,y} p(x,y) log(p(x|y)) \tag{2}$$

Let us now consider the Fano's inequality. Let us consider random variables, X and Y. Let us try to estimate X on the basis of Y. Let the estimate of X be the random variable $\hat{X}$, where $\hat{X} = g(Y)$. Here, g is a function of Y. We define the error probability P_e as $Pr(X \neq \hat{X})$. According to the Fano's inequality, the relationship between P_e and $H(X|Y)$ is:

$$H(P_e) \geq H(X|Y) - P_e(log(\mid \mathcal{X} \mid -1) \tag{3}$$

Here, $\mid \mathcal{X} \mid$ is the number of values that X can take. The values that X can take need to be from a discrete and finite set.

The greatness of the Fano's inequality is that it can be used to find the lower bound on the error that we will commit if we try to estimate the random variable X given another random variable Y. Here, Y can be the network activity of the last few epochs, and X can be the network activity in the next epoch. It is **not possible** to design a predictor that outperforms the Fano's bound. If we can demonstrate that method 1 has a better accuracy than the best possible accuracy (found with the Fano's inequality) of method 2, then method 1 is superior from an information theoretic point of view. It is important to note that the Fano's bound is dependent on $H(X|Y)$, or in other words the workload. Different workloads will have different Fano bounds.

Note that there is no known method of creating a predictor that achieves the Fano's bound. It is at the moment a theoretical tool that establishes a lower bound on the error, and an upper bound on the accuracy.

B. Evaluation of the Fano's Bound for Network Traffic

Let us now consider the case of a station that has a single core. Furthermore, let us assume a perfect epoch predictor. In this setting, let us consider the best address (PC based) predictor, $A25$, and all the link predictors in our arsenal. We choose the last 10 bits of the PC for the address predictor, and the behavior of the last 8 epochs for the link predictor. These are the best configurations for both the predictors respectively. We try to predict whether an epoch will transmit or not. This is a binary random variable. If we predict an L1 miss, then the epoch will transmit a flit for the address predictor. We do not consider responses to the directory or other cores in this study.

Figure 1 shows the results. The y-axis is the predictor hit ratio. For each bar, we have an error bar. The error bar shows the additional accuracy that can be theoretically achieved. The top of the error bar represents the Fano's bound.

The noteworthy point is that for 6 out of 10 benchmarks namely $barnes$, $blackscholes$, $radiosity$, $stencil$, $water\_nsq$, and $water\_sp$, the accuracy of $A25$ is more than the Fano's bound of all the link predictors. This means that irrespective of how good the link predictor is, its accuracy will always be lower than the address predictor, $A25$. If we consider the mean accuracy, then also the address predictor is better than the Fano's bound of all the other link based predictors.

For three of the remaining four benchmarks – fmm, fft, and $histo$ – $A25$ is convincingly inferior. However, in these benchmarks there is a relatively larger discrepancy between the Fano's bound and the actual accuracy achieved for $A25$. It might be possible to design better predictors. For $ocean$, the accuracy of $A25$ is better than the Fano's bound of L10, and is close to the Fano's bound of L50, which is the fastest link based configuration.

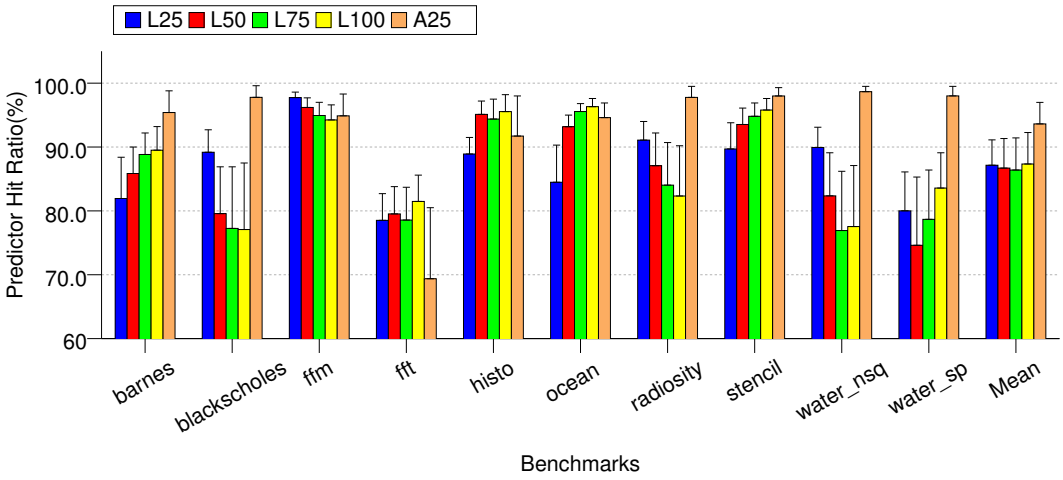

Figure 1. Predictor hit ratio and Fano's bound

Given the fact that in 7 out of 10 benchmarks, the accuracy of $A25$ is close or surpasses the Fano's bound of link predictors of interest, we believe that the PC based address trace is a better source of information.

APPENDIX B.
DIRECTLY MODULATED LASERS (DML LASERS)

There are two methods of modulating lasers: direct modulation and external modulation. In directly modulated lasers (DML Lasers), the laser itself is turned on and off. These are typically current injection lasers, and the input current is varied. Such lasers are typically low power lasers (less than 1W), and have a switching rate of 10-20 GHz. In comparison, externally modulated lasers do not modulate the laser itself. They have structures such as ring resonators, which absorb the laser power. They can switch at much higher frequencies (40-50 GHz), and can also deliver more power.

We are explicitly interested in directly modulated lasers. In Table I, we have shown a list of directly modulated lasers and corresponding parameters. Such lasers are commercially available (listed in Table I), and there are many research prototypes. Let us first discuss the research prototypes.

A. Research Prototypes

Faugeron et al. [12] proposed a high power, low relative intensity noise(RIN) directly modulated DFB laser with an output power of 140 mW at 550mA of input current. The wavelength of the laser is 1550nm. The modulation bandwidth is greater than 7GHz. It has a good electrical to optical conversion efficiency, 0.340W/A at 350 mA. Lasing starts at 80 mA. The working temperature is 25 degree Celsius. Other features are low noise and high linearity. Later Faugeron et al. [10] proposed a high optical power, high gain and high dynamic range laser with an output power of 180mW. The wavelength of operation is 1550 nm. It can be modulated at a frequency of 7.4GHz. The input power to the laser varies from 0 to 700mA. The maximum reported efficiency is 0.36 W/A at an output power of 136 mW. The laser is 1mm long. The linearity of the laser is also good.

Huang et al. [16] proposed an ultra high power, low RIN and narrow linewidth laser for 1550 nm DWDM communication. The maximum output power is 140mW and the input current varies from 0-400mA. The laser has an excellent RIN of -161dB and a narrow linewidth of 115kHz. The modulation frequency is between 2.5 and 40GHz. The efficiency is 63% at 80mW. The laser proposed by Burie et al. [7] is also an ultra high power and low RIN DFB laser. The maximum output power of the laser reaches 130mW with an input power of 1A. It has a high modulation frequency, 0.4-20GHz.

Another laser proposed by Loh et al. [18] is a packaged, high power, narrow linewidth, slab-coupled optical waveguide external cavity laser(SCOWECL). It has a maximum output power of 370mW at a wavelength of 1550nm. The modulation frequency varies from 200KHz to 10GHz. The coupling efficiency is a bit low and it is around 10%. The maximum input current needed is 4A and it shows maximum efficiency at 2A.

Recently, Faugeron et al. [13] proposed a high power, dilute mode DFB laser with tunable capacity. It has a maximum output power of 180mW and operates at 1550nm. The modulation frequency varies from 0.08-40GHz. The maximum input current is 550mA. The length of the laser is 1mm and the desired operating temperature is 25 degree Celsius.

B. Commercial DML Lasers

Directly modulated 1550 nm lasers are commercially available. We can use any of these lasers in our work. Table I

Research Proposals									
Name	Reference	Output Optical Power	Wavelength	Frequency	Slope Efficiency	Input variation	Remarks	Turn on delay(nS)	Wall plug efficiency
Faugeron et al.	[10]	180 mW	1550	7.4GHz	0.36 W/A @ 136 mW	0-700 mA	-	0.36	40% (5V, 90mA)
Faugeron et al.	[12]	140 mW	1550	7GHz	30-40% (best at 350mA, 0.98W)	0-600 mA	Lasing at 80 mA, 25 degree Celcius,	0.43	22%
Huang et al.	[16]	140 mW	1553	2.5-40Gbps	63% @ 80mW	0-400mA	25 degree celcius	0.27	63%
Burie et al.	[7]	130 mW	1545	20 GHz		1A		0.33	-
Loh et al.	[18]	370 mW	1550	200KHz - 10 GHz	10%	4A	Peak efficiency at 2A	2.07	6%
Faugeron et al.	[13]	180 mW	1550	0.08-40GHz		550mA	1mm long, 25 degree C, Tunable,	0.29	-
Chtioui et al.	[8]	100 mW		2-4GHz	25%	600 mA		0.40	-
Hou et al.	[15]	210 mW	1550			1A		0.32	-
Faugeron et al.	[11]	430 mW	1583	0-20GHz		3A		0.55	
Commercial Lasers									
Finisar DM80-01	http://www.finisar.com	30 mW	1527-1605	9.95-11.1GHz		200mA	Fixed power laser 25mA threshold current	0.40	
Finisar S7500	http://www.finisar.com	63 mW	1527-1568	10GHz		240mA	Tunable	-	10%
EMCore Medallion 8000	http://www.emcore.com	10 mW	1530-1560	2.8GHz		190mA		-	-
Fitel FOL15DDBA	http://www.furukawa.co.jp	10 mW	1550	2.5GHz	0.35 W/A	200mA		0.32	2%
3S Photonics 1.55m laser	http://www.3spgroup.com	10 mW	1550	32GHz	0.2 W/A	80mA		-	

Table I
PARAMETERS OF DIRECTLY MODULATED LASERS

lists a couple of such products. Some of these products are tunable lasers, where the output power can also be varied.

C. Thermal Stability

The frequency response of a directly modulated laser ($H(\omega)$) as well as the relaxation oscillation frequency (Ω_R) depend on temperature [24, 1, 25, 5]. There is a decrease of the relaxation oscillation frequency as well as in the peak of the $H(\omega)$ vs. ω curve as the temperature is increased, for a given value of injection current and threshold current [24].

The possibility of high temperatures in directly modulated lasers is reduced by employing thermo-electric coolers or water-based cooling, by spatially separating the laser and the driver circuitry, as well as by developing or mounting the laser on a thermally conducting semiconductor [22]. All of these methods have proved to be very successful in reducing the temperature variation in commercially available DML lasers. They are able to maintain a stable temperature profile as well as have negligible wavelength shifts across on and off states [22].

Recently uncooled directly modulated lasers have also demonstrated stable operation up to 100 °C at 25 Gbps [14].

D. Basic Physics

A laser can have three states during its operation. In the first state, the laser is completely turned off and no input current is supplied. The second state is a turned on state in which the laser produces optical output power. The third state is in between the first and second states in which the laser input current is not completely turned off but the laser does not produce any optical output. To change from state 3 to state 2, most lasers take less than 20-30 ps. But to move from a fully turned off to a fully turned on state, it takes more time.

The time taken by a laser to move from state 1 (fully turned off) to state 2 (turned on) is known as the *turn on delay*. The turn on delay of different lasers is shown in Table I. The turn on delay can be calculated using the following equation,

$$\tau_d = \tau_c \ln \frac{I_1}{I_1 - I_{th}} \tag{4}$$

Here, τ_c denotes the carrier lifetime, I_1 denotes the input current of the laser in state 2 and I_{th} denotes the threshold input current. The carrier lifetime of a material is in the order of a few nano seconds.

Our requirements are as follows. The total power dissipation of the laser was found to be typically less than 10W (including wall plug efficiency). Using a typical value of 30% as the wall plug efficiency, the optical power comes to roughly 3W. If we create an array of 32, 180mW lasers, we can deliver a peak optical power of 5.76W, which is sufficient for our purpose. Such laser arrays have been proposed before in the Probe and Pulse projects [26, 19].

We do not need to individually tune the lasers. We can create a step function like power gradient by turning on the requisite number of lasers. For example, if we want to supply $17/32^{th}$ of the peak power then we only turn on 17 lasers. We couple their power to an output waveguide, and send it to the chip. We can thus seamlessly support 32 power levels. Since modulating a laser requires less than 1 cycle (at 2.5 GHz), we are effectively using a tunable single cycle laser.

E. Conclusion

The **important point** to note from this discussion is that DML Lasers have been fabricated with an optical power output between 200-400 mW, turn on delay in the range of 0.2-0.5 ns, and modulation frequency in the range of 2-10 GHz.

We use a DML laser (similar to [10]) with a peak optical power of 5.76 W, and a turn on delay of 0.36 ns. With a clock speed of 2.5 GHz, we can modulate the laser in a single cycle.

APPENDIX C.
DETAILED EVALUATION

A. Configurations of Benchmarks

Application	Input size
PARSEC (simlarge)	
Blackscholes	64KB options
Bodytrack	4 cameras, 4 frames, 4,000 particles, 5 annealing layers
Splash-2	
Barnes	16KB particles
Fmm	16KB particles
Ocean	512 x 512 matrix (ocean contiguous)
Radiosity	batch, largeroom
Water_nsq	512 molecules (water nsquared)
Water_sp	512 molecules (water spatial)
Parboil	
Histo	256 x 8192 matrix
Stencil	512 x 512 x 64 3D matrix

Table II
CONFIGURATION OF BENCHMARKS

Table II shows the inputs of all the benchmarks from the Splash2 [23], Parsec [6] and Parboil [21] benchmark suites.

B. Station Activity Predictor Statistics

Table III shows the percentage of time we predict a station to be active, when it is actually inactive ($P(On|Off)$). We show data for all the benchmarks. The notable exception is fmm, which has a very low misprediction rate for address prediction. This is primarily because the PCs associated with irregular accesses are very nicely predictable. It is a relatively small set (less than 200 addresses).

Similarly, Table IV shows the percentage of time we predict a station to be inactive, when it is actually active ($P(Off|On)$) for all the benchmarks. Here, for also address prediction, fmm is the notable exception for the same reason.

C. Network Contention and NOC Activity

Figure 2 shows the degree of contention in the message queue(MQ) at the station controller (SC). The contention is measured in terms of cycles. On an average, the number of contention cycles is between 1-1.3 cycles across all the epoch sizes. The worst benchmark is fft in terms of contention (2.6 – 5.1 cycles). $histo$, fft, and $stencil$ have roughly 2 cycles of contention. Since the total amount of contention is limited to 1-2 cycles in most cases, we can conclude that the amount of contention is low.

Figure 3 shows the number of network messages per 1000 cycles for the entire system. The network per se is lightly loaded. On an average per cycle, we send 0.1 – 5 messages (mean 2.2 messages). The peak utilization is 20 messages per cycle. We can thus conclude that on an average the network utilization is 10% and contention is low. Keeping this in mind, we designed many of our protocols such as the design of the extra waveguide that work well when there is low contention.

D. Simultaneous Activity

Figure 4 shows the pdf of the number of stations that are simultaneously turned on for the $A25$ configuration. Similarly, Figure 5 shows the pdf for $L50$. For $A25$ we observe that the pdf gradually decays towards zero as the number of stations increase. Other than fmm and $ocean$, most benchmarks have 2-4 stations simultaneously active most of the time. In comparison, the pdf of the distribution has a much heavier tail for $L50$. There are peaks at 5, 13, and 19 stations. For $L50$, $histo$, $barnes$, and $radiosity$, which have a peak at 19-20 stations, are indeed the worst performing benchmarks in terms of power. Secondly, based on the distribution we can also understand why link activity based prediction systems consume 4X more power: they have more stations on simultaneously, and for longer durations.

APPENDIX D.
FAST TUNABLE SPLITTERS

A. Physics of Ring Resonators

A ring resonator is typically designed to resonate at a certain frequency. At this frequency it absorbs almost all the power from the through waveguide, and transfers most of it to the drop waveguide. The resonance condition is given by the Drude model.

$$\lambda_m = 2\pi R n_{eff}/m \tag{5}$$

Here, λ_m is the resonant wavelength, m is the mode (integer), R is the radius of the ring, and n_{eff} is the effective refractive index. The optical path length is defined as $2\pi R n_{eff}$. It should be an integral multiple of the resonant wavelength. From Equation 5, we can easily derive the following formula:

$$\frac{\Delta\lambda_m}{\lambda_m} = \frac{\Delta n_{eff}}{n_{eff}} \tag{6}$$

Once the wavelength of light starts to differ from the resonant wavelength by a large amount, all the power passes via the through port. The resonator stops acting like a splitter. Hence, to make a resonator work like a splitter, it is necessary to run it between its on and off states. The behavior of the resonator that is slightly off-resonance is captured by the Q factor. A resonator, with a high Q factor stops acting like a splitter for very small values of $\Delta\lambda$. Conversely, a resonator with a low Q factor acts like a splitter for a much larger range of $\Delta\lambda$. To make a resonator act like a splitter with a constant wavelength source, we need to change the optical path length. The microring is controlled in close proximity of the full-resonance. i.e The microring is used in the transient zone between resonance and off-resonance to perform as a splitter.

Benchmarks	Address				Link			
	25	50	75	100	25	50	75	100
barnes	2.17	1	0.63	0.28	14.91	7.16	3.88	2.22
blackscholes	11.27	11.51	13.76	10.99	6.45	10.49	16.25	18.01
fft	2.25	1.79	0.93	0.81	15.2	7.28	4.43	2.35
fmm	0.17	0.3	0.33	0.37	0.77	0.84	1.01	1.22
histo	1.11	0.18	0.09	0.05	4.05	1.31	2.6	3.6
ocean	2.27	1.36	0.39	0.31	7.64	3.33	1.88	1.31
radiosity	4.27	5.53	6.19	6.38	7	10.09	13.4	15.23
stencil	0.67	0.43	0.39	0.34	6.01	4.49	3.46	2.94
water_nsq	7.44	9.24	10.06	9.32	9.54	17.8	21.59	20.13
water_sp	5.93	6.11	5.86	4.62	13.02	17.73	16.88	11.88
Mean	3.755	3.745	3.863	3.347	8.459	8.052	8.538	7.889

Table III
PERCENTAGE OF TIME PREDICTED AS ACTIVE BUT ACTUALLY INACTIVE

Benchmarks	Address				Link			
	25	50	75	100	25	50	75	100
barnes	47.03	51.02	53.22	54.19	3.11	0.81	0.33	0.22
blackscholes	18.53	22.8	26.08	28.56	17.14	19.53	14.59	12.37
fft	44.62	50.31	52.29	53.58	3.49	1.7	0.59	0.32
fmm	3.12	4.57	5.54	6.66	1.8	2.82	3.36	4.03
histo	39.73	40.71	41.82	42.04	1.92	3.44	2.55	1.02
ocean	37.75	41.34	42.54	43.54	1.62	0.84	0.73	0.51
radiosity	20.06	21.74	22.53	23.56	12.68	15.89	14.13	13.06
stencil	29.39	32.54	33.44	34.15	2.46	0.97	0.86	0.87
water_nsq	22.17	22.94	24.49	27.75	16.1	17.18	10.11	6.98
water_sp	30.13	31.91	23.76	32.77	13.9	7.96	4.62	2.42
Mean	29.253	31.988	32.571	34.68	7.422	7.114	5.187	4.18

Table IV
PERCENTAGE OF TIME PREDICTED AS INACTIVE BUT ACTUALLY ACTIVE

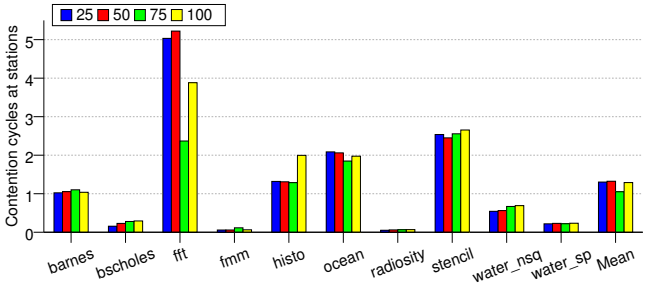

Figure 2. Contention cycles at stations

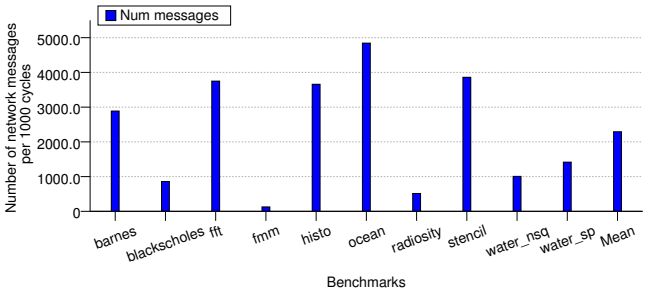

Figure 3. Number of network messages per 1000 cycles

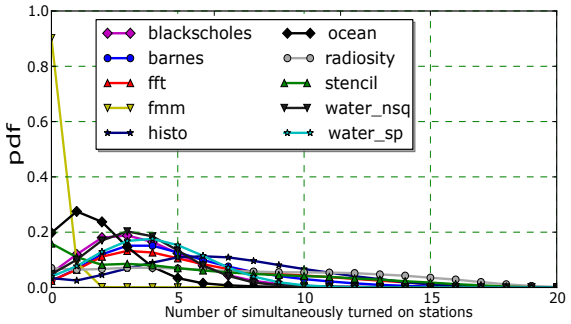

Figure 4. PDF of the number of stations turned on simultaneously (A25)

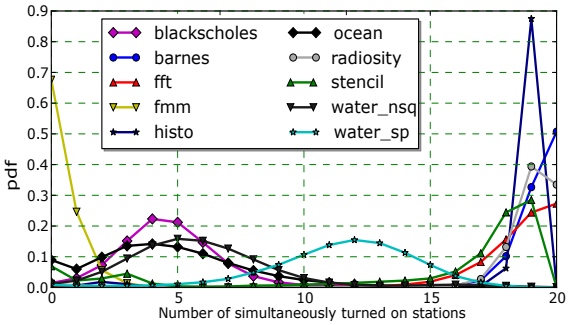

Figure 5. PDF of the number of stations turned on simultaneously (L50)

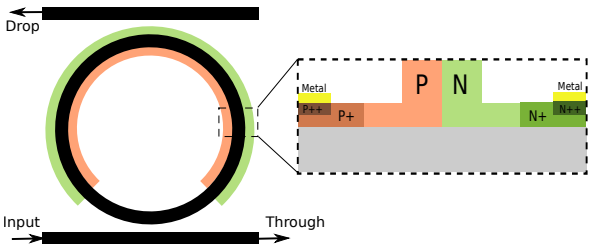

Figure 6. Schematic diagram of an active microring resonator

B. Electrically Tunable Ring Resonator

If we can vary the voltage applied to a part of the ring, we can alter the refractive index, and also the optical path length. If the optical path length is close to the resonant wavelength, the resonator will work like a splitter. Most nanophotonic ring resonators today use modulation voltages in the range of 1-3V [3]. To use the resonator as a splitter we need a fast DAC (digital to analog converter) that can produce any voltage between 0V and the modulation voltage. We already have commercially available 4-6 bit DACs that can switch at 2-5 GHz, which is enough for our purposes.

1) Design of an Active Ring Resonator based Splitter: In order to develop such a microring resonator modulator, modulation of the refractive index of the ring waveguide is carried out by employing several techniques. The most commonly used technique for fast switching is by actively controlling (i.e. by applying voltage) the carrier concentra-

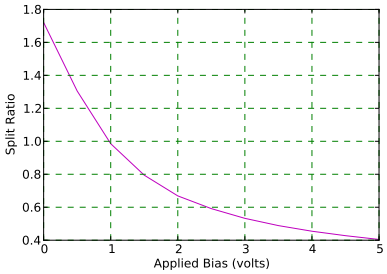

Figure 7. Split ratio of a microring resonator as a function of applied bias

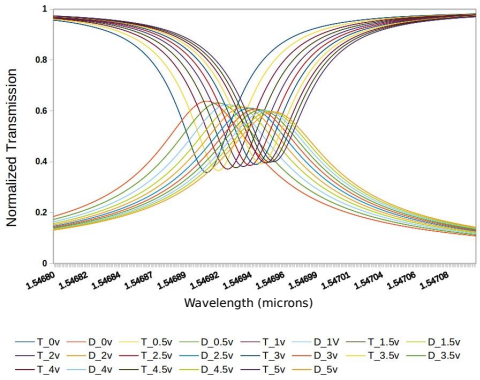

Figure 8. Shift in resonance wavelength in the through port and drop port with a change in applied voltage (*T*: Through port and *D*: Drop port)

tion in the ring waveguide. In a semiconductor, the carrier concentration has an impact on its refractive index. We employed a p-n junction based structure in the ring waveguide of the resonator and applied a reverse biased voltage to vary the depletion width of the junction (as illustrated in Figure 6). This is arguably a much faster technique compared to other mechanisms such as carrier injection in a p-i-n diode (proposed in [3]), because the movement of the carriers is limited by only its saturation velocity and the junction capacitance. Changes in the carrier density have also an effect on the Q factor of the ring as it influences the absorption.

We designed a ring resonator (slab thickness: 0.9 μm, rib thickness: 0.22μm, midpoint implant: 0, implant width: 0.22μm, radius: 9μm, width: 0.5μm), and simulated it with a reverse biased p-n junction device.

The designed microring resonator demonstrates a variation in split ratio on the application of biased voltage at a wavelength of 1548.91nm as shown in Figure 7. The voltage is varied from 0V to 5V to get a split ratio from 1.8 to 0.4. The important point to note is that we do have fair split ratios even at lower voltages. Figure 8 shows the resonant wavelength shift at the through and drop ports with respect to change in voltage. A DAC can be employed to generate the tuning voltage for this microring resonator [17, 20]. We can use such DACs to modulate the bias voltage at processor speeds ($\approx$ 2.5 GHz). Ring resonators are known to stabilize in less than a processor cycle [3] (100 ps in our experiments). Thus, the total tuning time is at the most limited to 1 cycle (@ 2.5GHz). We thus have a fast (near single cycle) ring resonator based tunable splitter.

C. Alternative Solutions using an Array of Resonators

1) Resonators of Different Sizes: Here also, the idea is the same. We operate a ring resonator in the transient region between the fully on and off states. In this region the resonator will pass a fraction of the power through the drop port. It will thus work like an optical power splitter. The

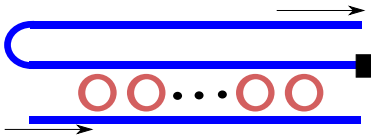

Figure 9. Schematic showing a 16-step tunable splitter

split ratio depends upon where we operate in the transient region. This in turn is influenced by the geometry of the ring resonator, especially the inner and outer radii. The idea is to use an array of 16 ring resonators with different geometries (and thus different split ratios), and enable only one of them at any point of time.

The design is shown in Figure 9. We use a set of high Q ring resonators of different sizes, where each of the resonators operates in the transient region and has a different split ratio. To make the array of 16 resonators work as a 16 step tunable splitter, we enable only one of the ring resonators out of 16. The rest of the resonators are in their off state, and let the optical signal pass through. The array thus works as a splitter. To change the split ratio, we enable the appropriate ring resonator in the array of resonators. Here, *enabling* means applying a voltage across the resonator p-i-n diode to appropriately bias it and change its optical path length such that it enters its transient region.

2) Resonators with Different Temperatures: Another practical method of achieving the same objective is to have resonators at different pre-set temperatures, instead of different geometries. We rely on the thermo-optic effect, which specifies that the rate of change of the refractive index with temperature is $1.86\times10^{-4}/K$. If we consider a 20K temperature tuning window, then we can change the refractive index by 0.003, and thus have an array of resonators operating at different temperatures, and consequently having different optical path lengths.

We can use the same technique as shown in Figure 9 to realize a 16-step tunable splitter. We can use micro-heaters to set the temperature of each resonator. Microheaters for ring resonators are already used in optical systems to maintain a steady temperature. If the separation(center to center) between two resonators is more than 4 μm, then the thermal coupling is very low [4, 9, 2].

Subsequently, we use the same approach. We enable 1 out of 16 resonators at any point of time to achieve a desired split ratio.

REFERENCES

[1] G. P. Agrawal, "Fiber-optic communication systems," *NASA STI/Recon Technical Report A*, vol. 93, p. 17972, 1992.

[2] K. Al-hemyari and C. T. Youtsey, "Localized thermal tuning of ring resonators," Oct. 21 2003, uS Patent 6,636,668.

[3] V. R. Almeida, C. A. Barrios, R. R. Panepucci, M. Lipson, M. A. Foster, D. G. Ouzounov, and A. L. Gaeta, "All-optical switching on a silicon chip," *Optics Letters*, vol. 29, no. 24, pp. 2867–2869, 2004.

[4] R. Amatya, C. W. Holzwarth, H. I. Smith, and R. J. Ram, "Precision tunable silicon compatible microring filters," *Photonics Technology Letters, IEEE*, vol. 20, no. 20, pp. 1739–1741, 2008.

[5] Y. An, A. Lorences Riesgo, J. Seoane, Y. Ding, H. Ou, and C. Peucheret, "Modulation speed enhancement of directly modulated lasers using a micro-ring resonator," in *1st IEEE Photonics Society Optical Interconnects Conference, OI*, 2012, pp. 32–33.

[6] C. Bienia, S. Kumar, J. P. Singh, and K. Li, "The parsec benchmark suite: characterization and architectural implications," in *PACT*, 2008.

[7] J.-R. Burie, G. Beuchet, M. Mimoun, P. Pagnod-Rossiaux, B. Ligat, J. Bertreux, J.-M. Rousselet, J. Dufour, P. Rougeolle, and F. Laruelle, "Ultra high power, ultra low rin up to 20 ghz 1.55 μm dfb algainasp laser for analog applications," in *OPTO*. International Society for Optics and Photonics, 2010, pp. 76 160Y–76 160Y.

[8] M. Chtioui, C. Feuillet, N. Massad, A. Vidal, J. Louardi, M. Faugeron, F. Van Dijk, M. Tran, Y. Robert, E. Vinet *et al.*, "Analog microwave photonic link based on a high power directly modulated laser, a high power photodiode and passive impedance matching," in *Microwave Photonics (MWP), 2012 International Topical Meeting on*. IEEE, 2012, pp. 269–272.

[9] P. Dong, R. Shafiiha, S. Liao, H. Liang, N.-N. Feng, D. Feng, G. Li, X. Zheng, A. V. Krishnamoorthy, and M. Asghari, "Wavelength-tunable silicon microring modulator," *Optics express*, vol. 18, no. 11, pp. 10 941–10 946, 2010.

[10] M. FAUGERON, M. Chtioui, A. Enard, O. Parillaud, F. Lelarge, M. Achouche, J. Jacquet, A. Marceaux, and F. van Dijk, "High optical power, high gain and high dynamic range directly modulated optical link," *Lightwave Technology, Journal of*, vol. 31, no. 8, pp. 1227–1233, April 2013.

[11] M. Faugeron, M. Krakowski, Y. Robert, E. Vinet, P. Primiani, J. Le Goëc, O. Parillaud, F. van Dijk, M. Vilera, A. Consoli *et al.*, "Monolithic master oscillator power amplifier at 1.58 μm for lidar measurements," in *International Conference on Space Optics*, vol. 7, 2014, p. 10.

[12] M. Faugeron, M. Tran, F. Lelarge, M. Chtioui, Y. Robert, E. Vinet, A. Enard, J. Jacquet, and F. Van Dijk, "High-power, low rin 1.55-directly modulated dfb lasers for analog signal transmission," *Photonics Technology Letters*, vol. 24, no. 2, pp. 116–118, 2012.

[13] M. Faugeron, M. Tran, O. Parillaud, M. Chtioui, Y. Robert, E. Vinet, A. Enard, J. Jacquet, and F. Van Dijk, "High-power tunable dilute mode dfb laser with low rin and narrow linewidth," *Photonics Technology Letters, IEEE*, vol. 25, no. 1, pp. 7–10, 2013.

[14] T. Fukamachi, K. Adachi, K. Shinoda, S. Tsuji, T. Kitatani, S. Tanaka, and M. Aoki, "Recent progress in 1.3-μm uncooled ingaalas directly modulated lasers," in *Semiconductor Laser Conference (ISLC), 2010 22nd IEEE International*. IEEE, 2010, pp. 189–190.

[15] L. Hou, M. Haji, J. Akbar, and J. H. Marsh, "Narrow linewidth laterally coupled 1.55 μm algainas/inp distributed feedback lasers integrated with a curved tapered semiconductor optical amplifier," *Optics letters*, vol. 37, no. 21, pp. 4525–4527, 2012.

[16] J.-S. Huang, H. Lu, and H. Su, "Ultra-high power, low rin and narrow linewidth lasers for 1550nm dwdm 100km long-haul fiber optic link," in *IEEE Lasers and Electro-Optics Society, 2008. LEOS 2008. 21st Annual Meeting of the*, Nov 2008, pp. 894–895.

[17] IDT, "Dac1653q/dac1658q quad 16-bit dac: 10 gbps jesd204b interface: x2, x4 and x8 interpolating," Tech. Rep., 2014.

[18] W. Loh, F. J. O'Donnell, J. J. Plant, M. A. Brattain, L. J. Missaggia, and P. W. Juodawlkis, "Packaged, high-power, narrow-linewidth slab-coupled optical waveguide external cavity laser (scowecl)," *Photonics Technology Letters, IEEE*, vol. 23, no. 14, pp. 974–976, 2011.

[19] R. Morris, E. Jolley, and A. K. Kodi, "Extending the performance and energy-efficiency of shared memory multicores with nanophotonic technology," *IEEE Trans. Parallel Distrib. Syst.*, vol. 25, no. 1, pp. 83–92, 2014.

[20] Semtech. (2014, April) Ultra-high speed adc and dac for advanced communication systems. [Online]. Available: http://www.semtech.com/Press-Releases/2014/

[21] J. A. Stratton, C. Rodrigues, I. J. Sung, N. Obeid, L. W. Chang, N. Anssari, G. D. Liu, and W. W. Hwu, "Parboil: A revised benchmark suite for scientific and commercial throughput computing," *Center for Reliable and High-Performance Computing*, 2012.

[22] B. Wohlfeil, L. Zimmermann, K. Petermann, J. Kreissl, and H. Gustat, "Thermal limits for integration of directly modulated lasers with driver ic on soi," in *Optical Fiber Communication Conference*. Optical Society of America, 2009, p. JThA34.

[23] S. C. Woo, M. Ohara, E. Torrie, J. P. Singh, and A. Gupta, "The splash-2 programs: characterization and methodological considerations," *SIGARCH Comput. Archit. News*, vol. 23, pp. 24–36, May 1995.

[24] T. Yamamoto, "High-speed directly modulated lasers," in *Optical Fiber Communication Conference*. Optical Society of America, 2012, pp. OTh3F–5.

[25] A. Yariv and P. Yeh, *Photonics: Optical Electronics in Modern Communications*, ser. The Oxford series in electrical and computer engineering. Oxford University Press, 2007.

[26] L. Zhou and A. K. Kodi, "Probe: Prediction-based optical bandwidth scaling for energy-efficient nocs," in *NOCS*, 2013.